SINGLE IMAGE LASER TRIANGULATION SYSTEM FOR 360° EXTERNAL INSPECTION OF CYLINDRICAL SHAPED OBJECTS USING INVERSE TRIANGULATION ALGORITHM

Sergio A. B. Petrovcic[1], Pedro D. V. Buschinelli[2], Marco A. M. Cavaco[2], Tiago L. F. C. Pinto[2*]

[1]LABAI Industrial Automation Laboratory – EEL, IFSC Federal Institute of Santa Catarina, Brazil.
[2]LABMETRO Metrology and Automation Lab – EMC, UFSC Federal University of Santa Catarina, Brazil

Technical Commission II

KEY WORDS: Inverse triangulation, Laser triangulation, 360° profilometry, Planar mirror, Optical metrology.

ABSTRACT:

This paper proposes a new Laser Triangulation System (LTS) that allows an 360° external inspection for each acquired image using two planar mirrors, one laser line projector, and one camera. The new measurement algorithm is based on the inverse triangulation in which the analysis is made from 3D object space to image space, the opposite of traditional LTS algorithms, with laser peak detection in favourable directions even in an image with multiple reflections of the object. Measurement system principle, calibration and metrological evaluation are described based on simulated experimental data and 3D reconstructions examples. Uncertainty for a 20 mm plain plug gauge measurement was ±0.07 mm for 95.45% confidence.

1. INTRODUCTION

Inspecting external surfaces of long cylindrical shaped objects in 360°, such as wire ropes, is a challenging task. Some traditional approaches, like using multiple sensors around the object, a rotatory table with one sensor, or a single sensor moving around the object, are generally not feasible or are too complex to implement. Planar mirrors are commonly used to increase the field of view (FoV) of optical systems instead of duplicating other hardware, like cameras, for example. Shape-from-silhouette (Forbes et al., 2006) was successfully used for 3D reconstruction of small objects, but at least two images with four virtual objects are needed. The same occurs to contour-based (Po-Hao Huang e Shang-Hon Lai, 2006), although only one image is needed with four virtual objects. Stereo triangulation with fringe projection (Lanman, Crispell and Taubin, 2007) also successfully reconstructed small objects, but it requires two cameras and a fringe projector with sequential acquisitions with orders of magnitude slower than an LTS. A stereo laser triangulation system able to reconstruct objects surfaces in 360° using a Micro-Electro-Mechanical Systems (MEMS) laser scanner and two cameras was proposed by (Jin et al., 2017). (Li, Kästner and Reithmeier, 2018) developed an edge sensor using one prism, two planar mirrors, two laser projectors, and one camera to measure with an over 180° FoV. In traditional algorithms for LTS, the laser line peak is first detected in the image plane, acquired by a calibrated camera allowing tracing rays from the camera optical centre. The interception of these rays with the previously calibrated laser plane represents the reconstructed object surface along the laser line (Santolaria et al., 2009). Thus, in these algorithms, the analysis is made from image space to 3D object space.

To the best of the authors' knowledge, there is no work describing a system able to perform a 360° external surface inspection using only one laser triangulation sensor in a single camera shot. This paper proposes a new LTS design and algorithms that allow an 360° external surface inspection using two planar mirrors, one laser line projector, and one camera. A complete 360° external section is measured for each acquired image. Also, the new measurement algorithm introduced in this paper is based on the inverse triangulation in which the analysis is made from 3D object space to image space, inverting the logic of the traditional LTS algorithms.

The inverse triangulation algorithm changes 3D points determination, switching from image-oriented to object-oriented analysis. The classical triangulation algorithm starts in image space by detecting pixels that meet a criterion followed by estimate the 3D point in object space. The inverse triangulation works the opposite way, starting with a set of 3D points in object space followed by the analysis of the image pixels. In addition, some advantages arise compared to the classical triangulation algorithm. The density of the resulting point cloud can be controlled directly in object space by the space between each 3D point in a regular grid, allowing to control the computation load and the point cloud density. In the case of a laser triangulation system, the search for the laser line peak centre naturally occurs perpendicularly to the laser line. This characteristic is even more evident in a system that uses multiple reflections in the mirrors for a 360° measurement.

Some researchers have successfully used similar algorithms with stereo and fringe projection systems (Hofmann, 2006)(Pinto et al., 2010)(Buschinelli et al., 2016) and multiple cameras with image correlation (Haertel et al., 2015), but this work presents for the first time an inverse triangulation based algorithm for laser triangulation. This work proposes a new Laser Triangulation System (LTS) that allows an 360° external inspection of cylindrical shaped objects. Each acquired image using two mirrors, one laser projector, and one camera is processed with a new measurement algorithm based on the inverse triangulation applied to an LTS.

* Corresponding author: tiago.pinto@ufsc.br

2. THEORY REVIEW

2.1 Pinhole camera model

The pinhole camera model is used in the developed system. In this model, a camera intrinsic matrix $\boldsymbol{K}$ is expressed by:

$$K = \begin{bmatrix} f_x & \gamma & u_0 \\ 0 & f_y & u_0 \\ 0 & 0 & 1 \end{bmatrix} \qquad (1)$$

where $f_x = \frac{f}{d_x}$, $f_y = \frac{f}{d_y}$ and $c = [u_0 \quad v_0]^T$.

In equation (1), f represents the focal length of the camera, f_x and f_y are the camera focal length in pixels in x and y directions, d_x and d_y are the distance between consecutive pixels centres, γ is the skew between x and y sensor axes (typically zero, since pixels deviation to a right angle is neglectable), and c is the centre of the image. The projection matrix $\boldsymbol{P}$ projects a given 3D point in object coordinates into the image plane in camera coordinates. It can be expressed as:

$$P = K\,[\,I \mid 0\,]\begin{bmatrix} R & t \\ 0 & 1 \end{bmatrix} = K\,[\,R \mid t\,] \qquad (2)$$

Where $\boldsymbol{R}$ and t are, respectively, the rotation matrix and translation vector from object to camera coordinate system, which are the extrinsic parameters. The camera lens distortion can be compensated using Brown´s model (Brown, 1971) considering radial and tangential distortions. The camera can be calibrated using, for example, the *Camera Calibration Toolbox for Matlab* (Bouguet, 2006).

2.2 Planar mirror model

A planar mirror may be represented by a plane, with normal $\mathbf{n}$ and distance d from the camera centre (Gluckman and Nayar, 1998). The mirror transformation matrix T_π is given by:

$$T_\pi = \begin{bmatrix} (I_3 - 2\mathbf{n}\mathbf{n}^T) & 2d\mathbf{n} \\ 0_{1x3} & 1 \end{bmatrix} \qquad (3)$$

where I_3 is a $3x3$ identity matrix. A planar mirror works as a symmetry plane, where a 3D symmetry line passing through the real and virtual points is perpendicular to the mirror (a). Even more, as shown in Figure 1(b), the epipolar line in an image acquired by a camera is the projection of the 3D symmetry line of a reflected point (François, Medioni and Waupotitsch, 2003).

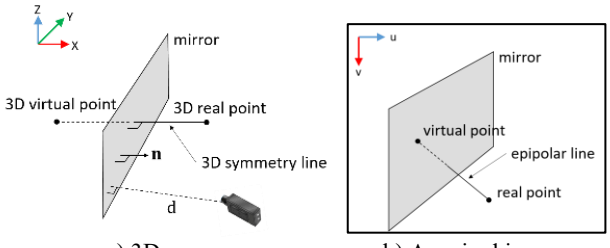

a) 3D scene. b) Acquired image.

Figure 1: Real point mirrored in a planar mirror.

A calibration must be performed to obtain the mirror orientation and its distance from the camera. Some approaches can be adopted, such as using autocalibration (Forbes et al., 2006), marking on object and a ruler (I-Chen Lin, Jeng-Sheng Yeh and Ming Ouhyoung, 2002), putting four rounded marks on mirror and knowing the distance between at least two marks (Jang, Lee and Jung, 2004), having a planar chessboard positioned over the mirror (Lanman, Crispell and Taubin, 2007), and having a mirror with lithographic chessboard (Zou, Wei and Liu, 2019).

2.3 General inverse triangulation principle

The basic inverse triangulation algorithm was introduced in (Hofmann, 2006) to measure the inner surface of pipes with a stereoscopic system (using two cameras with conic lenses) with fringe projection and a cylindrical coordinate system. Another stereoscopic system with fringe projection was also used by (Pinto et al., 2010), but this time with cartesian coordinate system, to measure free form surfaces. (Haertel et al., 2015) used three cameras and digital image correlation to measure the inner surface of pipes. An underwater stereoscopic system based on fringe projection through flat refractive interfaces using cartesian coordinate system was developed by (Buschinelli et al., 2016).

Figure 2 shows a stereoscopic system with object-oriented 3D points mesh in a cartesian coordinate system. This regular grid is created according to the desired measurement volume and density by choosing the appropriate resolutions (δ_x, δ_y, δ_z) and range. In the object space, for each XY pair, all Z values are tested (scan in Z direction) by mathematically projecting each tested 3D point on each camera image plane with the camera projection matrix P. Each projected point is now tested based on some criterion. If the current pixel or interpolated subpixel position meets the criterion, such as the same phase value for fringe projection (Pinto, 2010), the corresponding 3D point is considered valid and it is stored as an object 3D point; otherwise the point is removed.

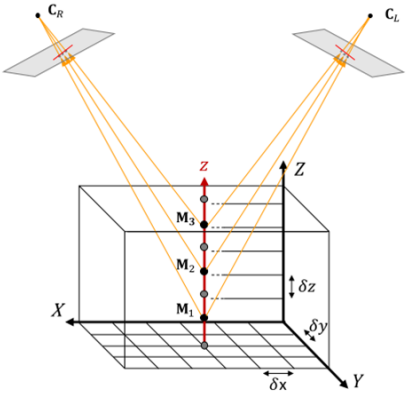

Figure 2: Inverse triangulation. Three different 3D points are tested for a specific XY coordinate in the regular grid. The cube represents the measurement volume with resolutions δ_x, δ_y and δ_z (Buschinelli et al., 2017).

Unlike classical triangulation algorithm, the density of the resulting point cloud can be controlled by the space between each 3D point in the regular grid, allowing to control the computation load and the point cloud density. Additionally, the 3D point cloud is organized in the coordinate system of choice that best suits the type of object been measured, e.g., cartesian, polar or cylindrical.

3. PROPOSED SYSTEM

3.1 360° laser triangulation system

This work proposes a new Laser Triangulation System (LTS) that allows an 360° external inspection of cylindrical shaped objects for each acquired image. It is composed of two mirrors, one laser

line projector, and one camera. Figure 3 show the proposed LTS using two first surface planar mirrors π_L and π_R mounted with an angle β of 90°, one diode laser plane projector, and a camera mounted with a triangulation angle α of 40°. Figure 4 shows an isometric view of the proposed system, in which the front part of the object is captured directly by the camera and the rear part of the object is captured by the right and left virtual image generated by the mirrors completing the 360° view of the cylindrical object illuminated by the laser line illustrated by a synthetic image. Laser line and mirrors must be carefully aligned to avoid multiple reflections.

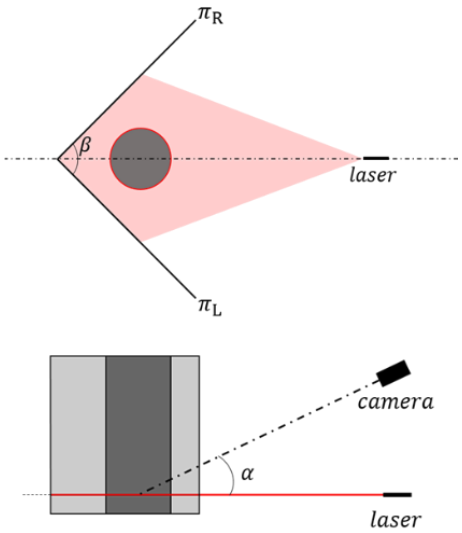

Figure 3: Schematic top and lateral view of the proposed LTS for 360° acquisition in one image.

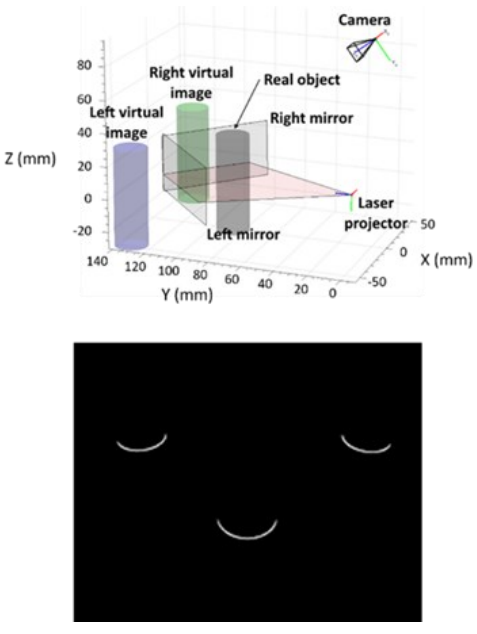

Figure 4: Isometric view of the proposed 360° LTS and a simulated acquired image.

3.2 Inverse triangulation for 360° LTS

The inverse triangulation algorithm changes the 3D points determination. Organized and predefined 3D points in a convenient coordinate system are mathematically projected on the image plane and the intensity information on these image points are analysed to define the best 3D points between candidates. The inverse triangulation switches from image-oriented to object-oriented analysis. In addition, some advantages arise compared to the classical triangulation algorithm: (a) The density of the resulting point cloud can be controlled in object space, defining space between each 3D point in a regular grid, and (b) the search for the laser line peak naturally occurs perpendicularly to the laser line. This characteristic is even more evident in a system that uses multiple reflections in the mirrors for a 360° measurement of cylindrical shaped objects as described in this work.

For a calibrated system, i.e., calibrated camera, laser plane, and mirrors, a cylindrical coordinate system is defined aligned to the laser plane where the axis of the cylindrical object should be placed. The cylindrical coordinate system is used for convenience due to object's shape. For a regular grid defined in the object´s space cylindrical coordinate system, a point cloud of 3D points in homogenous coordinates is created with radial and angular range and step defined by the user. This 3D point cloud is then mirrored and/or projected in the image space. The left and right mirrors transformation matrixes (T_π^{left} and T_π^{right}) are applied to the regular grid, mirroring the 3D points. Now there are three regular grids: one for the real object and two mirrored for the left and right virtual objects. A general formula may be expressed as shown below, where $\tilde{G}$ are 3D points and $\tilde{g}$ are image plane points represented in homogeneous coordinates. In the case of the real object regular grid, the mirror transformation matrix T_π should be replaced by a 4x4 identity matrix.

$$\tilde{g} = P * T_\pi * \tilde{G} \qquad (4)$$

The measurement itself can now be performed. The intensity of each point projected in the image space is evaluated with subpixel accuracy using cubic interpolation. For each discretized angle (between $\theta_{mín}$ and $\theta_{máx}$ with step $\delta\theta$), the scan along the radius is executed (R_{scan}), as shown in Figure 5. Each discretized radii array is evaluated based on the centroid algorithm (Tang *et al.*, 2009) to detect the laser line centre. A threshold filter may be used prior to centroid algorithm to remove background noise. Once the centre is found, the associated 3D point for this radial direction is valid and all other 3D points are discarded. The angle of the radial direction tested is increased and a new scan is performed. A known relative movement can be done in the Z axis to scan the cylindrical object.

Figure 5 summarizes the inverse triangulation algorithm, in which the 3D point cloud to be tested is defined in the object space and then projected in the image space for the front view and is mirrored and projected in the image space for the rear views. For each radial direction, the projected 3D points are evaluated to find the laser peak. The 3D point associated with laser peak is considered valid and a part of the measured section. For each view in the image plane, a suitable range in the radius and radial direction can be chosen to restrict the search. Figure 6 shows an example of the laser peak detection and a real measured section result.

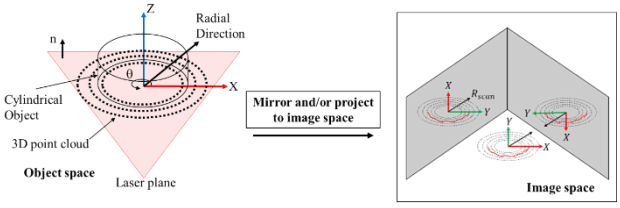

Figure 5: Object space 3D point cloud definition and mirroring/projection to image space.

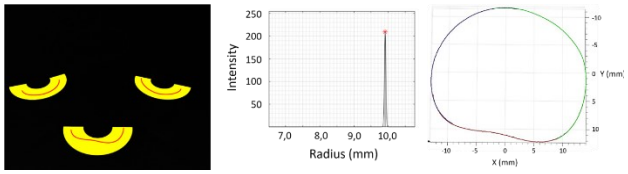

(a) (b) (c)

Figure 6: (a) 3D point cloud projected in a real image space (yellow) and detected peaks (red), (b) peak detection for a radial direction, and (c) a reconstructed section of a real object with a single image, with red points for the front view and blue and green points for mirrored views.

4. EXPERIMENTAL RESULTS

This section describes the system setup and the main calibrations steps before the measurement uncertainty evaluation as well as several examples of measured objects.

4.1 Experimental setup

The experimental setup is shown in Figure 7. It consists of a *Ximea* monochrome camera model xIQ MQ013MG-E2 with 1280 x 1024 pixels resolution and 8-bit depth equipped with an 8 mm focal length Computar lens model M0814-MP2 2/3" (A), a 660 nm 1 mW Coherent laser line projector (B), and two first surface mirrors (C and D). A linear positioning stage was used to control the Z axis step between measured sections (E). The angle between mirrors was set to 90°. The laser projector fan angle is 50°. The triangulation angle between laser plane and camera optical axis is about 40°.

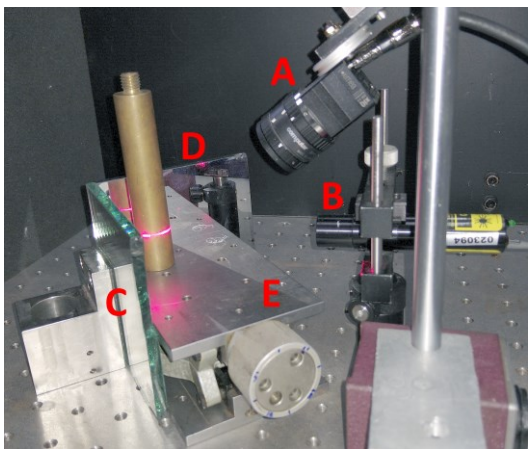

Figure 7: LTS system setup a) camera and lens, b) laser line projector, c) left and d) right first surface mirrors, and e) vertical translation table.

4.2 Mirror calibration

After camera calibration, mirrors and laser planes are calibrated. To calibrate both the mirrors and laser projector, due to the restricted space, a small chessboard pattern of 7x6 squares of 2 mm was created, printed as a sticker, placed over a 3 mm thick glass, and calibrated using the Quick Vision machine from Mitutoyo. Images with the chessboard pattern in different positions and orientations were captured, assuring that the calibration pattern was visible both directly by the camera and through the mirror. For each image, the *Camera Calibration Toolbox for Matlab* (Bouguet, 2006) is used to find the 3D coordinates of the real and virtual chessboard patterns in camera coordinate system, allowing the determination of the mirror plane (images with large reprojections errors are discarded). Figure 8 left shows the chessboard corners detected at the real and virtual chessboards while Figure 8 right shows the 3D symmetry lines. For each pair of real and virtual 3D point, the mean value is computed. All the mean points are used to best fit a plane, which is the mirror plane. The mirror normal and location are used to compute the mirror transformation matrix.

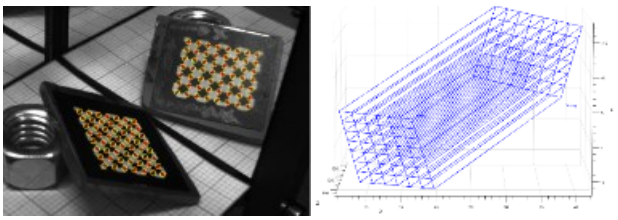

Figure 8: Left: Chessboard corners detected at the real and virtual chessboards, and Right: 3D symmetry lines.

4.3 Laser plane calibration

With the same chessboard pattern used to calibrate the mirrors, images with the chessboard pattern in different positions and orientations were captured with the laser on and off, adjusting the camera exposure time, as shown in Figure 9. The process used is similar to (Li, Kästner and Reithmeier, 2018).

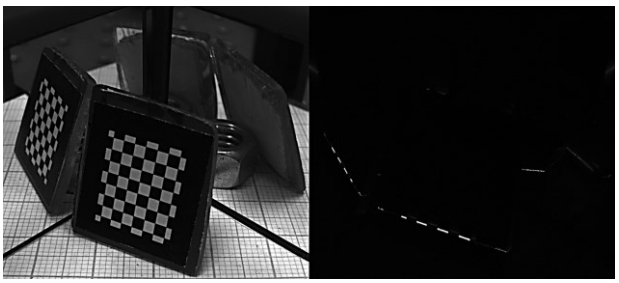

Figure 9: Calibration images with laser off and on.

The intersection of the laser sheet on the chessboard pattern results on a laser line. The line centre is detected using the centroid algorithm. Rays starting from the camera optical centre passing through the detected points are created. The *Camera Calibration Toolbox for Matlab* (Bouguet, 2006) is used to find the 3D coordinates of the real chessboard pattern. Next, a plane representing the chessboard pattern plane is fitted. The 3D coordinates of the laser line are found by the intersection of the rays with the chessboard pattern plane. Therefore, the laser sheet can be computed fitting a plane to all laser line 3D points because all these points should belong to the same plane. At least two different positions of the chessboard pattern are needed since infinite planes can be fitted if all points are collinear.

4.4 Compensating residual errors

To compensate for possible residual errors, a section of a cylinder with small shape error was measured. The main factor of a residual misalignment between points from different reflections is probably a mirror calibration residual error. To compensate for this error, a circle is fitted to each point cloud and its centre is computed. The translation vector of each reflected fitted centre to the front side fitted centre is computed and used to refine the alignment. The measurement uncertainty evaluation and measurement examples used this alignment refinement.

4.5 Measurement uncertainty evaluation

To evaluate the system accuracy, a plain plug gauge of (19.9987 ± 0.0004) mm diameter was measured. Figure 10 shows the acquired image for the gauge placed at central position. This gauge was measured ten times for the approximately same place. Each time the gauge was placed an image was captured and then removed. Figure 10 shows an example of acquired image. The mean radius length error of all measurements is 0.015 mm. Considering the worst-case radius error standard deviation of 0.025 mm, a gauge diameter variation due to a 5°C temperature change of ± 0.0003 mm and the resolution of 0.001 mm, the resulting combined expanded Uncertainty is ±0.05 mm with 95,45% confidence. Considering the tendency and the expanded uncertainty, the maximum statistical error for measurement of the 20 mm diameter plain plug gauge is ±0.067 mm.

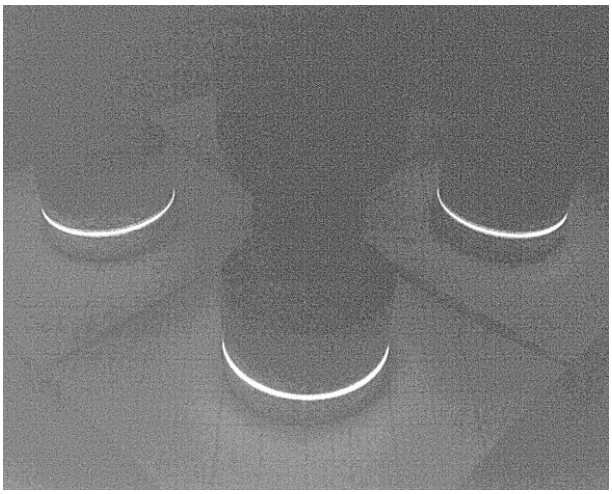

Figure 10: Plain plug gauge acquired by the LTS camera. Image adjusted for a better view.

4.6 Measurement examples

Examples of measured objects and the respective measured 3D point cloud, with red points for the front view and blue and green points for mirrored views, are shown from Figure 11 to Figure18, ranging from cylindrical objects to wire cables and other shapes. The red region signalized in some objects indicates the measured area.

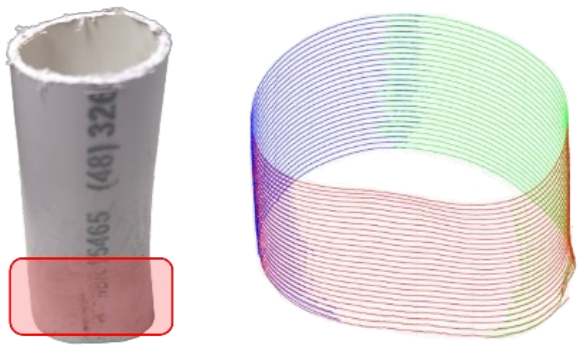

Figure 11: 1” deformed PVC pipe – 26 measured sections with 0.68 mm displacement between sections.

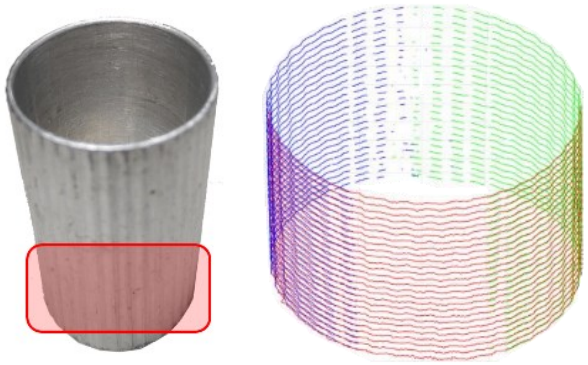

Figure 12: 22 mm diameter aluminium pipe with undulations – 26 measured sections with 0.68 mm displacement between sections.

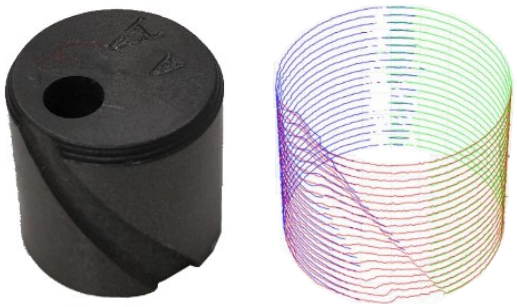

Figure 13: 13 mm diameter steel shaft with black oxidation and helical groove – 20 sections with 0.68 mm between sections.

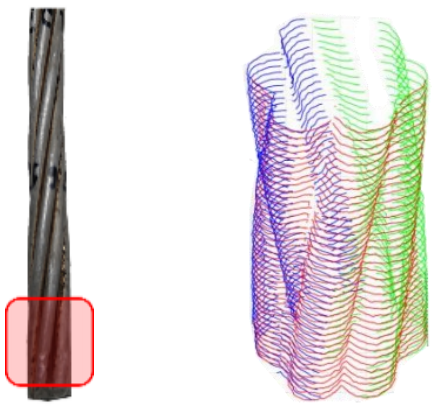

Figure 14: 6 mm diameter aluminium distribution cable – 40 sections with 0.34 mm between sections.

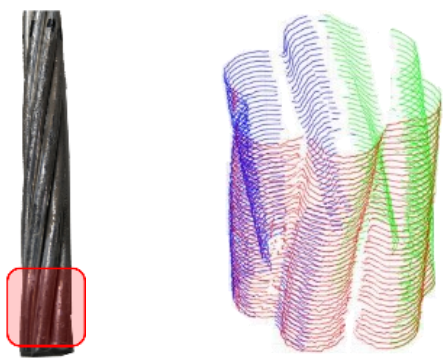

Figure 15: 8 mm diameter aluminium distribution cable – 39 sections with 0.34 mm between sections.

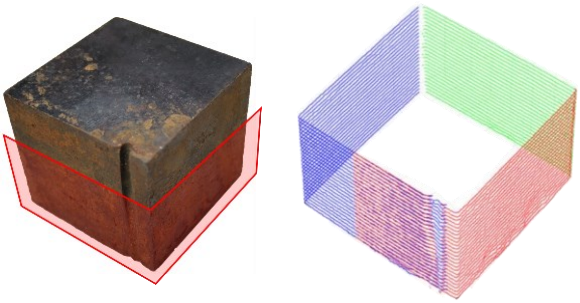

Figure 16: 28 mm rusty cube with groove – 25 sections with 0.68 mm between sections.

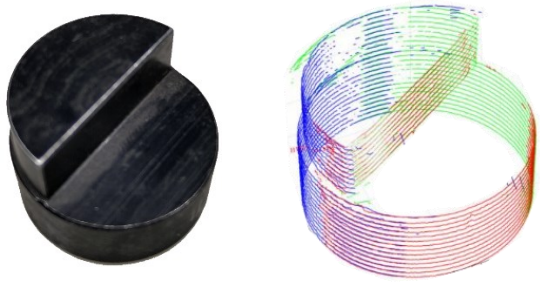

Figure 17: 25 mm diameter cylindrical shaft with undercut – 25 sections with 0.68 mm between sections.

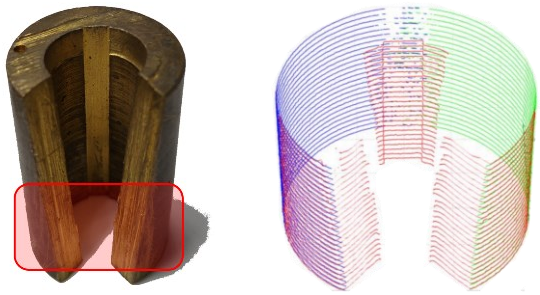

Figure 18: 25 mm diameter hollow brass cylinder with diagonal cut – 25 sections with 0.68 mm between sections.

4.7 Discussion

The proposed system successfully reconstructed external surfaces of cylindrical shaped objects ensuring overlap between the views. Cable shaped objects, due to its complex shape, were reconstructed but with some occlusions, as expected. Other shaped objects were also successfully reconstructed with a good overlap between sections. The measurement of the plain plug gauge has shown that the system has a ±0.07 mm measurement maximum error. The object's surface finish influences the measurement quality. Objects with white and/or opaque surface had better results while shiny and specular surfaces lead to poor measurements.

5. CONCLUSIONS

A 360° external surface reconstruction system with only one laser triangulation sensor was presented in this paper. By using only one camera and one laser line projector with two planar mirrors, the system can perform a 360° external surface reconstruction of cylindrical shaped objects. This makes the proposed system simple and powerful compared to other systems. A full 360° section can be measured using only a single image. To the best of our knowledge, there is no such system in literature.

The hardware setup allows excellent overlap between the views. For complex shaped objects, some occlusions may occur. The maximum measurement mean error of the system is ±0.07 mm. The object's surface finish influences the measurement quality. When measuring cylindrical shaped objects, inverse triangulation associated with a cylindrical coordinate system allows the scanning of the laser line centre preferably perpendicularly to the line, minimizing errors. The main advantages, compared to the classical triangulation algorithm, are the regular point cloud with point density control, the possibility to use any coordinate system, the computation load control, and the possibility to measure parts instead of the entire object.

ACKNOWLEDGEMENTS

We gratefully acknowledge Elsio Varela for setting up some experiments, LabAI (Industrial Automation Laboratory) of Federal Institute of Santa Catarina (IFSC), Labmetro (Metrology and Automatization Laboratory) of Federal University of Santa Catarina (UFSC), and CERTI Foundation (Centros de Referência em Tecnologias Inovadoras).

REFERENCES

BOUGUET, J.-Y. 2006: Camera Calibration Toolbox for Matlab, Open Source. (24 October 2022) http://robots.stanford.edu/cs223b04/JeanYvesCalib/

BROWN, D. C. 1971: Close-range camera calibration. *Photogramm Eng*. (24 October 2022) https://www.asprs.org/wp-content/uploads/pers/1971journal/aug/1971_aug_855-866.pdf

BUSCHINELLI, P. D. V. et al. 2016: Underwater 3D shape measurement using inverse triangulation through two flat refractive surfaces. *OCEANS 2016 MTS/IEEE Monterey*. DOI: 10.1109/OCEANS.2016.7761231 http://ieeexplore.ieee.org/document/7761231/

FORBES, K. et al. 2006: Shape-from-Silhouette with Two Mirrors and an Uncalibrated Camera. *In: European Conference on Computer Vision (ECCV 2006)* p. 165–178. https://link.springer.com/chapter/10.1007/11744047_13

FRANÇOIS, A. R. J.; MEDIONI, G. G.; WAUPOTITSCH, R. 2003: Mirror symmetry⇒2-view stereo geometry. *Image and Vision Computing*, v. 21, n. 2, p. 137–143. https://doi.org/10.1016/S0262-8856(02)00149-X

GLUCKMAN, J., & NAYAR, S. K. 1998: A real-time catadioptric stereo system using planar mirrors. *In Proc. of Image Understanding Workshop* (p. 7). (24 October 2022) https://cave.cs.columbia.edu/old/publications/pdfs/Gluckman_IUW98.pdf

HAERTEL, et al. 2015: Trinocular stereo system with object space oriented correlation for inner pipe inspection. *Measurement.* Volume 73, Pages 162-170. https://doi.org/10.1016/j.measurement.2015.05.015

HENRI HOFMANN, A. C. 2006: Stereoscopic endoscopic optical system for 3D measurement of pipeline welded unions' internal geometry. *Proceedings - SPE Annual Technical Conference and Exhibition*, v. 7, n. Student 7, p. 5039–5043. https://doi.org/10.2118/106523-STU

I-CHEN LIN; JENG-SHENG YEH; MING OUHYOUNG. 2002: Extracting 3D facial animation parameters from multiview video clips. *IEEE Computer Graphics and Applications*, v. 22, n. 6, p. 72–80.]
https://doi.org/10.1109/MCG.2002.1046631

JANG, K. H.; LEE, D. H.; JUNG, S. K. 2004: A moving planar mirror based approach for cultural reconstruction. *Computer Animation and Virtual Worlds*, v. 15, n. 34, p. 415–423.
https://doi.org/10.1002/cav.45

JIN, R. et al. 2017: A novel 360-degree shape measurement using a simple setup with two mirrors and a laser MEMS scanner. *Unconventional and Indirect Imaging, Image Reconstruction, and Wavefront Sensing 2017*.
https://www.spiedigitallibrary.org/conference-proceedings-of-spie/10410/2276854/A-novel-360-degree-shape-measurement-using-a-simple-setup/10.1117/12.2276854.full

LANMAN, D.; CRISPELL, D.; TAUBIN, G. 2007: Surround Structured Lighting for Full Object Scanning. *Sixth International Conference on 3-D Digital Imaging and Modeling (3DIM 2007)*.
http://ieeexplore.ieee.org/document/4296745/

LI, Y.; KÄSTNER, M.; REITHMEIER, E. 2018: Triangulation-based edge measurement using polyview optics. *Optics and Lasers in Engineering*, v. 103, n. November 2017, p. 71–76.
https://doi.org/10.1016/j.optlaseng.2017.11.015

PINTO, T. et al. 2012: Regular mesh measurement of large free form surfaces using stereo vision and fringe projection. *Optics and Lasers in Engineering* Volume 50, Issue 7, Pages 910-916.
https://doi.org/10.1016/j.optlaseng.2012.03.003

PO-HAO HUANG; SHANG-HON LAI. 2006: Contour-Based Structure from Reflection. *IEEE Computer Society Conference on Computer Vision and Pattern Recognition* - Volume 1 (CVPR'06).
http://ieeexplore.ieee.org/document/1640783/

SANTOLARIA, J. et al. 2009: Modelling and Calibration Technique of Laser Triangulation Sensors for Integration in Robot Arms and Articulated Arm Coordinate Measuring Machines. *Sensors*, v. 9, n. 9, p. 7374–7396.
https://doi.org/10.3390/s90907374

TANG, S. et al. 2009: Improved iteration centroid algorithm based on linear CCD light-spot location. *9th International Conference on Electronic Measurement & Instruments*.
http://ieeexplore.ieee.org/document/5274043/

ZOU, Wei; WEI, Zhengzhong; LIU, Fulin. 2019: High-accuracy calibration of line-structured light vision sensors using a plane mirror. *Optics Express* 27, 34681-34704
https://doi.org/10.1364/OE.27.034681